The Astronomical Journal, 151:127 (13pp), 2016 May
doi:10.3847/0004-6256/151/5/127

LIMITATIONS OF CN AND CH MOLECULAR BAND STRENGTHS AT HIGH METALLICITIES: A CASE STUDY IN NGC 6791

Owen M. Boberg[1], Jeffrey M. Gerber[1], Eileen D. Friel[1], Sarah Martell[2], Michael M. Briley[3], and Heather L. Morrison[4]
[1] Department of Astronomy, Indiana University, USA
[2] School of Physics, University of New South Wales, Australia
[3] Department of Physics and Astronomy, Appalachian State University, USA
[4] Department of Astronomy, Case Western Reserve University, USA
Received 2015 September 10; accepted 2016 January 6; published 2016 May 3

ABSTRACT

We present an analysis of the CN and CH molecular band strengths in NGC 6791 from low-resolution Sloan Extension for Galactic Understanding and Exploration spectra as a means to detect chemical variations in the cluster. NGC 6791 is a heavily studied open cluster (OC) due to its unique combination of old age, high mass, and high metallicity. These characteristics place NGC 6791 between the physical properties of most globular and OCs. Recent photometric and spectroscopic studies yield contradicting results, with some claiming to detect signs of multiple populations, as in globular clusters, while others do not. We do not find large spreads in the CN and CH band strength distributions that would suggest multiple populations. By pairing spectral synthesis with the measured CN values, we conclude that the maximum [N/Fe] variation in the cluster is 0.2 dex. Additionally, we find that the saturation of the CH band at high metallicities limits its usefulness in detecting multiple populations and determining C abundances.

Key words: globular clusters: general – open clusters and associations: general – open clusters and associations: individual (NGC 6791) – stars: abundances

1. INTRODUCTION

Being among the oldest and most massive open clusters (OCs) in the Milky Way (MW), NGC 6791 has been a heavily studied and debated cluster. Early color–magnitude diagram (CMD) ages of NGC 6791 ranged from 6 to 12 Gyr, depending on the stellar evolutionary models and reddening assumed for the cluster (Anthony-Twarog & Twarog 1985). Similarly affected by these assumptions, the [Fe/H] of NGC 6791 has ranged from approximately solar to [Fe/H] $\sim +0.44$ (Friel & Janes 1993; Tripicco et al. 1995; Peterson & Green 1998). Today, it is more widely accepted that NGC 6791 is indeed one of the oldest (∼7–9 Gyr, King et al. 2005; Brogaard et al. 2012), most metal-rich ([Fe/H] $= +0.4$, Gratton et al. 2006), and most massive OCs in the MW ($\sim 10^4 M_\odot$, Liebert et al. 1994; Platais et al. 2011), making it a unique member of our Galaxy's OC system. These characteristics make NGC 6791 a suitable environment to study the relationship between OCs and the low-mass MW globular clusters (GCs), as well as test our definitions as to what distinguishes the two.

In recent years, the presence of an Na–O anticorrelation has been used as a defining characteristic of GCs (Gratton et al. 2012). In all but the least massive GCs, spectroscopic studies have found that most MW GCs exhibit an Na–O anticorrelation and other light-element abundance variations indicative of a not-so-simple star formation history. It is thought that these chemical signatures require a high enough cluster mass to retain processed material that is used to produce a secondary generation of stars that is chemically distinct from the primordial generation. The interplay between cluster mass and the presence of the Na–O anticorrelation is illustrated extremely well by Figure 3 of Carretta et al. (2010). In that figure the authors plot the absolute *V* magnitude of a sample of GCs and OCs, as an indicator of mass, versus their respective relative ages. The clusters in this diagram that have been found to exhibit the Na–O anticorrelation are distinguished from those that do not; none of the clusters with a mass below $4 \times 10^4 M_\odot$ exhibit the Na–O anticorrelation. Although there are only two clusters observed below this mass limit, the authors suggest that $\sim 4 \times 10^4\ M_\odot$ could be the minimum mass needed for a cluster to exhibit an Na–O anticorrelation. This lower mass limit falls very close to the mass of NGC 6791, providing further motivation to use this cluster as a means to study the boundary between OCs and GCs.

To explore this boundary, recent photometric and spectroscopic studies of NGC 6791 have focused on determining if it shows characteristics of chemically distinct populations of stars, similar to what is observed in GCs. A photometric study of NGC 6791 by Twarog et al. (2011) found that the spread in the turn-off region of the CMD is wider than could be explained by differential reddening, photometric errors, and the binary sequence in the cluster. Twarog et al. (2011) suggest instead that the spread in the CMD is indicative of an extended period of star formation in NGC 6791, lasting on the order of 1 Gyr. This point is contested, however, by Platais et al. (2011), who find that differential reddening is driving the scatter and spread observed in the CMD. Additionally, photometric studies find that there are several extreme blue horizontal branch stars present in the cluster, which is not typical at such a high metallicity, or in OCs (Kaluzny & Udalski 1992; Liebert et al. 1994; Peterson & Green 1998; Platais et al. 2011). These photometric features suggest that NGC 6791 has gone through an evolution that is not typical of OCs, and could possibly include the formation of multiple generations of stars.

The spectroscopic studies of NGC 6791 have also produced interesting and debated results. Geisler et al. (2012) found that there are two distinct groups of Na abundances among NGC 6791 members. Stars in these two groups have about the same O abundance and do not follow the trends seen in

GCs. This was the first time this phenomenon was observed in an OC and suggested multiple populations. Using low-resolution Sloan Digital Sky Survey (SDSS) spectra, Carrera (2012) determined the molecular band distributions in NGC 6791 and concluded that the CN band strength distributions are significantly wider than errors on their measurements, indicating the presence of light-element variations in the cluster. A study by Hufnagel et al. (1995) came to a similar conclusion about the molecular band strengths in NGC 6791. Recently, however, additional high-resolution studies have presented a contradictory picture. Bragaglia et al. (2014) and Cunha et al. (2015) measured abundances for a large sample of cluster members and do not detect an Na–O anticorrelation or variations in other light elements in the cluster that are larger than the expected observational errors.

Collecting high-resolution spectra for a large number of stars in NGC 6791 is difficult due to its large galactocentric distance and the sparsity of bright stars near or along the red giant branch (RGB). Using low-resolution spectra to measure the molecular CN and CH band strengths, however, provides an additional method to search for chemical inhomogeneities and has been used extensively in both early and recent studies of GCs (see Kraft 1994; Gratton et al. 2012 and references therein). The positive correlation of Na abundance with N abundance, which in turn correlates with CN band strength, allows the tracing of the Na-poor and Na-rich populations with the CN-normal and CN-strong populations, respectively. The strength of these molecular bands is, however, also dependent on the surface gravity, temperature, and metallicity of a star, and to evaluate the presence of light element variations within the cluster, one compares the distribution of band strengths within a given evolutionary stage to the typical error on their measurement.

In this study, we will present an additional analysis of the CN and CH molecular band strengths in NGC 6791 and discuss these results in the context of other spectroscopic studies. In Section 2 we will present the data used in our study and the overlap between our data set and the previous spectroscopic studies. In Section 3 we will define the indices used to measure band strengths and describe the various techniques used to characterize their distributions. In Section 4 we will explore the behavior of the CN and CH molecular band strengths in NGC 6791 and as a function of [Fe/H] with the help of synthetic spectra. We will conclude with a discussion of the limitations of molecular band strength analysis at high metallicities and how these limitations affect what one can conclude about NGC 6791.

2. DATA

The spectra used in our study were collected as part of the Sloan Extension for Galactic Understanding and Exploration (SEGUE; Yanny et al. 2009). NGC 6791 and a number of other GCs and OCs were observed to serve as calibration targets for the SEGUE Stellar Parameter Pipeline. In Figure 1 we plot the V versus B–V CMD for NGC 6791 from Stetson et al. (2003). Marked on the CMD are the stars that are in the SEGUE sample, their assigned evolutionary state, and the stars that are in both the SEGUE sample and/or one of the recent high-resolution studies: Bragaglia et al. (2014), Cunha et al. (2015), and Geisler et al. (2012). The SEGUE spectra have $R \sim 2000$ and range from 3800 to 9200 Å. It can be seen from the CMD that interloping field stars may be mis-identified as cluster members, so careful selection of our sample was important. We used the membership criteria described in Morrison et al. (2016): radial velocities, proper motions, and position on the CMD. Carrera (2012) used an independent membership determination, but our sample nearly completely overlaps with that study.

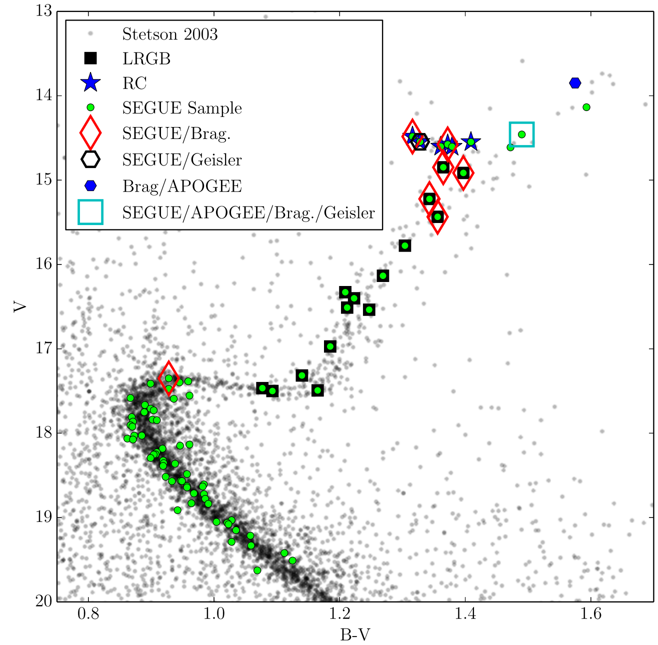

Figure 1. V vs. B–V CMD marking the stars in the SEGUE sample and those stars also observed in high-resolution studies.

3. CN AND CH BAND STRENGTH ANALYSIS

3.1. Band Index Definitions

In order to measure the molecular band strength in a given spectrum, one typically takes the ratio of the integrated flux in a spectral window containing the molecular band feature to the integrated flux in a reference spectral window that does not. For our band strength analysis we used the $S(3839)_N$ band as defined by Norris et al. (1981), the $CH(4300)_L$ band as defined by Lee (1999), and the $S(4142)$ band as defined by Norris & Freeman (1979). These band definitions were chosen because they are used in a survey of molecular band strengths in GCs by Smolinski et al. (2011) and are the definitions used by Carrera (2012). The $CH(4300)_L$ band has also been used over a large range of metallicities, which will become relevant later on in the discussion. The definitions of the three bands are given in Equations (1)–(3). It should be noted that there are a number of different band definitions that can be used for these measurements, but they are typically tuned to one specific cluster or metallicity (see Martell et al. 2008):

$$S(3839)_N = -2.5 \log \frac{\int_{3846}^{3883} I_\lambda d\lambda}{\int_{3883}^{3916} I_\lambda d\lambda} \quad (1)$$

$$S(4142) = -2.5 \log \frac{\int_{4120}^{4216} I_\lambda d\lambda}{\int_{4216}^{4290} I_\lambda d\lambda} \quad (2)$$

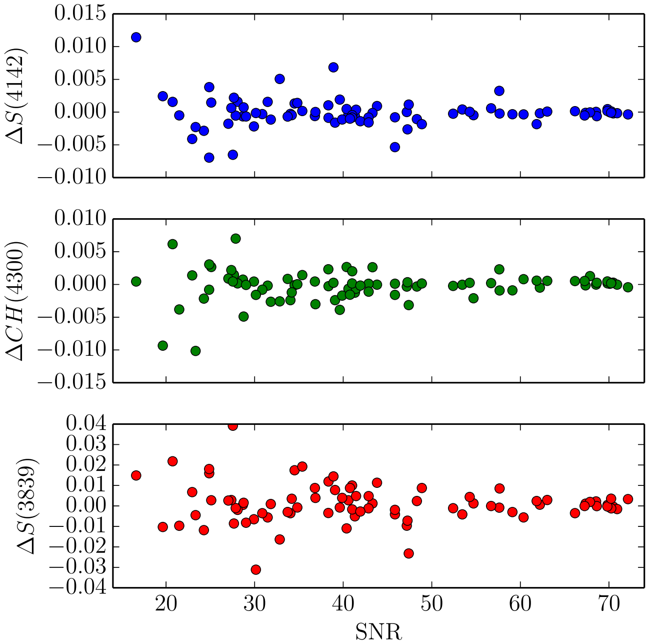

Figure 2. Difference in band strength Δ as calculated by `IDL INT_TABULATED` and a trapezoid rule with non-uniform step sizes vs. signal-to-noise ratio (S/N) for stars in the NGC 6791 sample.

$$\mathrm{CH}(4300)_\mathrm{L} = -2.5 \log \frac{\int_{4270}^{4320} I_\lambda d\lambda}{\frac{1}{2}\left(\int_{4230}^{4260} I_\lambda d\lambda + \int_{4390}^{4420} I_\lambda d\lambda\right)}. \quad (3)$$

To integrate the flux in the spectral windows given in the equations, we used a trapezoid rule with non-uniform step sizes. In calculating these band strengths, we found that the method of numerical integration can result in differing band strengths on the order of several hundredths of a magnitude. The differences between the methods increase with decreasing signal-to-noise ratio (S/N) of the spectra. This effect contributes an additional source of uncertainty to calculating these band strengths that may not have been realized in previous studies. In Figure 2 we plot the difference between the three band strengths as calculated by the `IDL INT_TABULATED` routine and our method, versus the S/N of the spectra where the bands were measured. These differences become the largest below an S/N of ~40. Comparing the widths of the band strength distributions, given in the final column of Table 1, we find that the differences in integration technique are generally much smaller than the spread in measurements except at the lowest S/N for $\mathrm{CH}(4300)_\mathrm{L}$.

3.2. Pseudo Indices

To characterize the CN and CH distributions in NGC 6791, the sample of stars was first divided by evolutionary state based on their location in the V versus B–V CMD in Figure 1. Since we expect the indices to vary with evolutionary state and luminosity, we will first divide the sample by evolutionary state and then model their variation with V magnitude or (B–V) color. For the main-sequence (MS) and RGB stars we then plotted their band strengths versus V magnitude as shown in Figures 3–5. The source of the error bars will be discussed in detail in the next subsection. We then fit a linear relationship to the $\mathrm{S}(3839)_\mathrm{N}$, $\mathrm{S}(4142)$, and $\mathrm{CH}(4300)_\mathrm{L}$ band strengths with the V magnitude, which is plotted as a red line in the figures. A linear fit was chosen to follow the convention of previous molecular band strength studies. By calculating the vertical distance of each $\mathrm{S}(3839)_\mathrm{N}$, $\mathrm{CH}(4300)_\mathrm{L}$, and $\mathrm{S}(4142)$ measurement from the linear fit, we form a pseudo-index denoted by a "δ." The pseudo-index serves as a band strength measurement that is independent of the differences in luminosity and temperature among the stars along the MS and RGB. A similar process is followed for the red clump (RC) stars except the band strengths are plotted versus their (B–I) color. It is in the distribution of these pseudo-indices that we look for signatures of multiple populations through large spreads in the chemical abundances. This technique has been used in many of the previous molecular band strength studies of GCs.

3.3. Index Errors

It is also important to quantify our errors carefully so that we can evaluate whether we are seeing true variation in CN or CH at a given luminosity and evolutionary state. To assign errors to our band strengths, we used a Monte Carlo method. Noise was added to each pixel in the spectra by drawing a number from a normal distribution with a standard deviation equal to the standard deviation in that pixel as reported by the SDSS pipeline. The band strengths were then measured with the noise-added spectra, and the process was repeated 1000 times. The standard deviation of these 1000 Monte Carlo runs was then assigned as the error on the band measured.

An issue with this method is that it can underestimate the errors (Martell & Grebel 2010). To account for this underestimate, the Monte Carlo errors are typically multiplied by an integer smoothing factor N so they are similar to the errors reported in other studies. For example, the typical uncertainty on the $\mathrm{S}(3839)_\mathrm{N}$ band is ~0.05 mag (Smolinski et al. 2011), so the Monte Carlo errors are usually smoothed so they are no less than that value. In the other bands, however, there is not a consensus on what the typical errors should be. The error bars on Figures 3–5 are the unsmoothed errors resulting from this Monte Carlo method.

The errors and this smoothing factor are crucial to what conclusions one can draw from the band strength distributions because they determine the width of the Gaussian kernels used to generate generalized histograms of the band strengths. Each pseudo-band measurement is treated as a Gaussian with a standard deviation equal to the error in its measurement. The individual Gaussians are then added together to produce a generalized histogram. Doing this creates a continuous distribution of pseudo-band strengths that can be examined for substructure, and it can be determined whether it is wider than is expected based on the errors. If the errors and the smoothing factor are too small, they will introduce structure in the distributions that is not really there, such as multiple peaks. If the smoothing factor is too large, it could erase real substructure in the distributions and hide signs of large abundance spreads.

3.4. Testing Different Smoothing Factors

We used three different methods to determine the size of the smoothing factor that was applied to the individual errors. The simplest of these methods was multiplying the errors by an increasing integer factor. For our second method, we determined the smoothing factor based on the rms of the

Table 1
Median Errors from Different Methods

Molecular Band	Monte Carlo MC	Scaling rms[a]	Optimal Kernel Width O.K.W	Width of Gaussian Fit σ_{Fit}	Carrera Gaussian Fit $\sigma_{\mathrm{Carrera}}$
$S(3839)_N$(MS)	0.04	0.08	0.06	0.08	0.083
$S(3839)_N$(RGB)	0.03	0.07	0.03	0.09	0.083
$S(3839)_N$(RC)	0.01	0.05	0.02	0.05	0.053
$CH(4300)_L$(MS)	0.01	0.02	0.01	0.01	0.045
$CH(4300)_L$(RGB)	0.01	0.01	0.01	0.02	0.031
$CH(4300)_L$(RC)	0.004	0.008	0.002	0.009	0.02
S(4142) (MS)	0.01	0.02	0.01	0.02	0.046
S(4142) (RGB)	0.01	0.02	0.02	0.02	0.037
S(4142) (RC)	0.003	0.02	0.02	0.013	0.03

Note.
[a] rms of pseudo-indices (δ) in each sample.

pseudo-band strength values within an evolutionary stage. If the Monte Carlo error on a given band strength measurement was less than the rms of that pseudo-band strength sample, the individual error was multiplied by an integer so it would be no less than the rms. This method, however, could also artificially erase structure that is present in the distribution.

With our final method, we sought to determine if there was a way to calculate the optimal kernel width based on the distribution of the individual measurements. To do this, we used threefold and leave-one-out cross-validation to do a grid search over different kernel width values. For this technique, the kernel width of the individual Gaussians was assigned to a subset of the band strength measurements that acted as a training data set. A kernel density estimate (KDE) is then generated based on the training data. It is then determined how well those data not included in the training data set are fit by the resulting KDE, and the value of the kernel width is assigned a score based on the quality of the fit. The process is then repeated over the entire grid, and the kernel width with the highest score is the optimal value for the KDE. By comparing this optimal kernel width with those produced by multiplying the Monte Carlo errors by some smoothing factor, we can get a sense of how well the smoothed Monte Carlo errors represent the band strength distributions.

3.5. CN and CH Distributions

In the second and third columns of Figures 3–5 we plot the generalized histograms of the $\delta CH(4300)_L$, $\delta S(3839)_N$, and $\delta S(4142)$ indices in the MS, RGB, and RC samples, respectively. In the second column of each figure there are a set of generalized histograms that were created with various smoothing factors as determined by the three methods described in the previous subsection. The different curves are labeled based on the width assumed in creating them. The unsmoothed errors from the Monte Carlo method are labeled as "MC." Curves that were generated with integer multiples of the Monte Carlo errors are labeled as "NMC," where *N* will be replaced with the integer used (i.e 2MC, 4MC). The curve generated using the rms scaling method is labeled as "RMS," and the curve generated using cross-validation to determine the optimum kernel width is labeled as "O.K.W."

In the third column of each figure, we plot the generalized histogram resulting from the unsmoothed Monte Carlo errors as a solid line with a Gaussian fit to the distribution plotted as a dashed line. The points in each of the plots in this column have error bars with lengths equal to the median error used in creating the generalized histogram they represent. They are labeled in the same fashion as their respective curves in the second column. This was done to allow for a comparison of the typical errors in each generalized histogram with the width of the single Gaussian fit to the MC curve. We also list these values in Table 1. These figures clearly show that the method used to determine the errors in the band strengths, and what (if any) smoothing factor is applied to those errors, greatly affects the conclusions one would draw from them. This is especially true for the RC sample in each of the bands. The CN and CH distributions in this sample show the most structure if one does not apply a smoothing factor. This structure, however, is much more likely to be caused by the small sample rather than true structure in the distributions. The *y*-axis of the RC histograms shows that there are only two or three stars in each of the bins, and in some cases as few as one. This illustrates how much the apparent structure in these distributions is driven by small numbers.

In the final column of Table 1 we list the standard deviation of the single Gaussian fit to each band strength distribution as found by Carrera (2012). The widths of the $S(3839)_N$ distribution in our study and Carrera (2012) are in good agreement for every evolutionary stage. In the other bands, however, Carrera (2012) finds Gaussian fits that are wider than ours. All of the stars from Carrera (2012) were also included in our sample, so that is not likely to be the source of the differences between the studies. The method of how the spectra are interpolated to the edge of the spectral windows, the numeric integration technique used to measure the flux in each band, and differences in the linear fit used to defined the pseudo-indicies, however, could cause variations in the final distributions and their respective Gaussian fits.

3.6. CN and CH Anticorrelation

If the variations in CN strength in NGC 6791 are due to abundance variations in the cluster, one might expect to see CN strengths anticorrelated with CH strengths. In moderately low metallicity GCs with abundance variations, this anticorrelation is indeed seen as one CH strong and CN weak population, and the other CN strong and CH weak (Smith 1987; Briley et al. 1992; Kraft 1994).

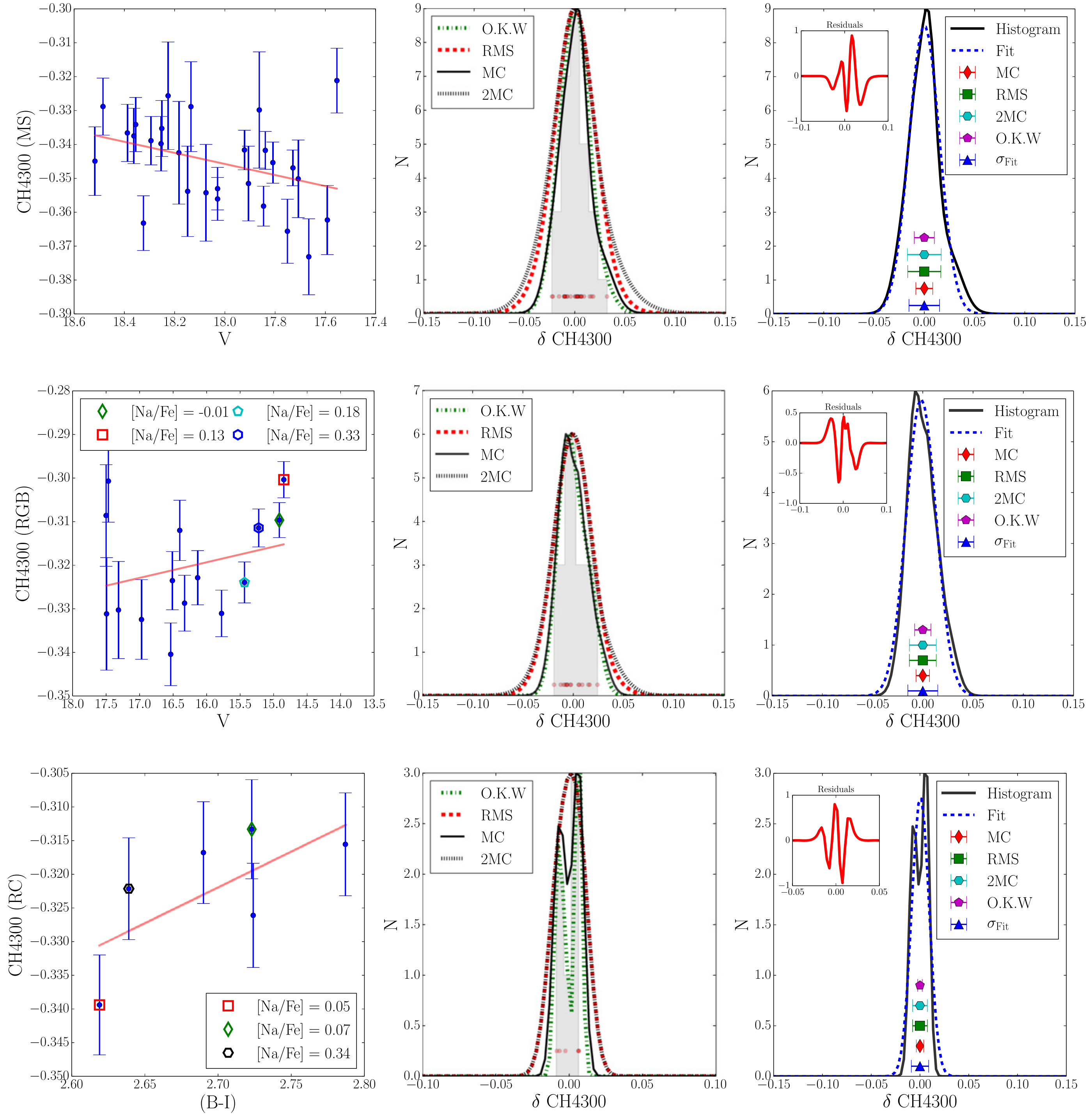

Figure 3. Determination of the δCH(4300)$_{\rm L}$ indices and their generalized histograms. In the first column the band strengths are plotted vs. their V magnitude or color. The red line is the linear fit used to calculate the pseudo-indices. In the middle column we plot the generalized histograms resulting from assuming different errors. Also plotted are the binned histograms, shaded in gray. MC is the unsmoothed Monte Carlo error, and NMC is an integer multiple of the MC error, such as 2MC. The errors determined from the optimal kernel width technique and rms scaling are labeled as O.K.W, and RMS, respectively.

To see if this anticorrelation is present in NGC 6791, we followed the method used in Smolinski et al. (2011) of plotting the CH(4300)$_{\rm L}$ index versus δS(3839)$_{\rm N}$ and δS(4142) as shown in Figure 6. As a comparison, we also make these plots for RGB stars in the GCs M3 and M15 in the bottom row of Figure 6. The data for M3 and M15 were taken from Smolinski et al. (2011). M3 nicely illustrates the separation of the two populations and the anticorrelation between their CH and CN strengths. M15 illustrates the limitation of this analysis at low metallicities; the CN distribution is unimodal, and the CH distributions shows an extended tail rather than distinct populations. From the high-resolution studies by Carretta et al. (2009), however, we know that there are indeed multiple populations present in M15 as indicated by its Na–O anticorrelation. At low metallicities, like those in M15, it is too difficult to detect the variations in band strengths that would

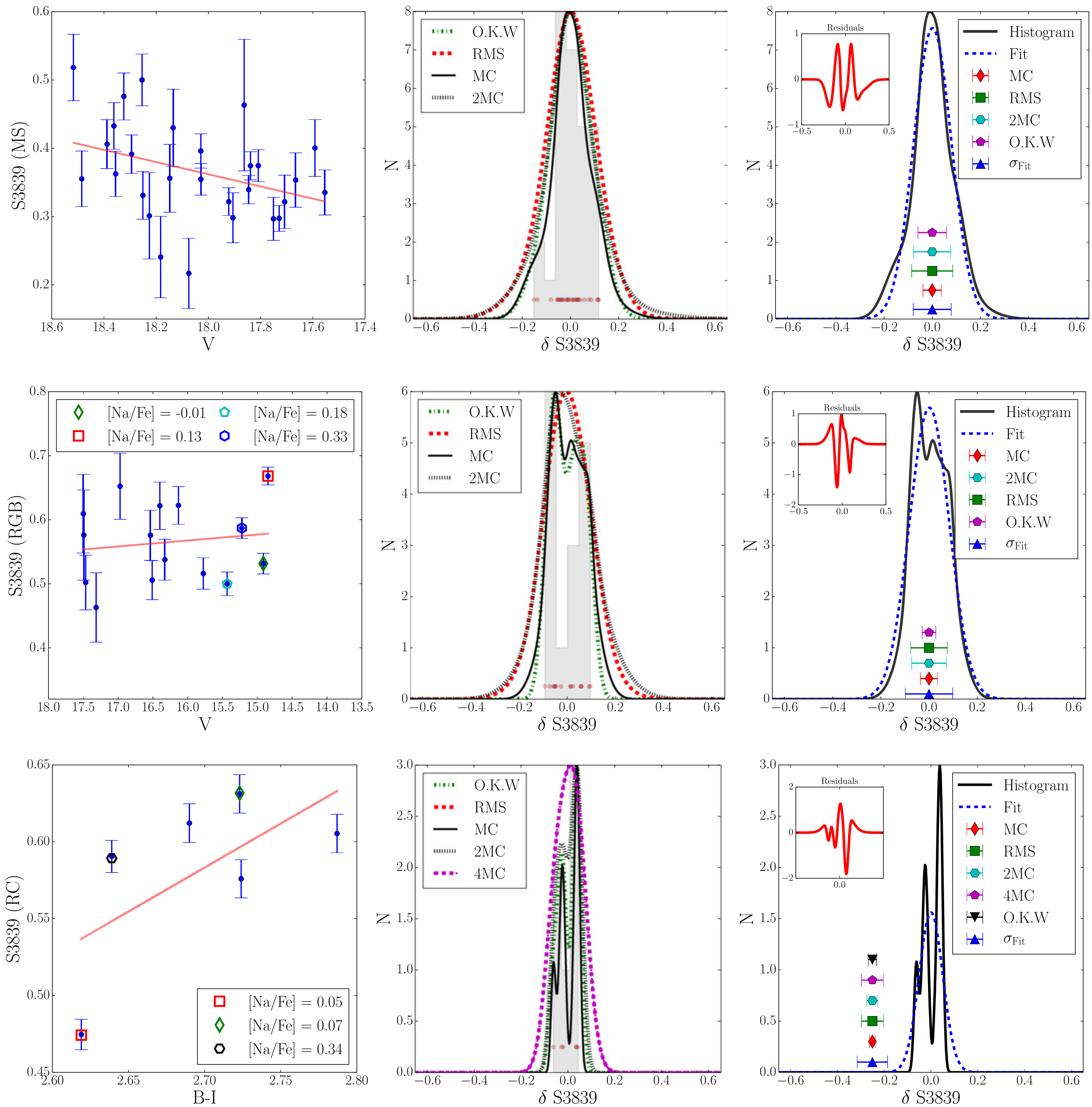

Figure 4. As in Figure 3, but for the $\delta S(3839)_N$ indices.

indicate multiple populations (see Shetrone et al. 2010; Smolinski et al. 2011). In the final panel of the last row in Figure 6, we plot the $CH(4300)_L$ versus $\delta S(3839)_N$ in NGC 6791 RGB stars over a range of values equivalent to those in the M3 and M15 plots. From this panel, we see that there is no clear separation of CN-normal and CN-strong stars, nor a clear anticorrelation between CN and CH band strength over the typical ranges seen in GCs. This lack of anticorrelation in NGC 6791 could be a result of no chemical variations in the cluster, or the limitation of this type of analysis at high metallicities. We explore the latter case in the following section.

4. ABUNDANCES FROM HIGH-RESOLUTION WORK

The work by Geisler et al. (2012) provided the first evidence of an OC (NGC 6791) showing signs of chemical inhomogeneities among its members that appeared not to be driven by stellar evolution. Those findings, however, have not been confirmed by other recent high-resolution spectroscopic studies of NGC 6791 (Bragaglia et al. 2014; Cunha et al. 2015). These two most recent studies have provided Na, O, C, and N abundances for cluster members; those members in common with our SEGUE sample are shown in Figure 1. We note that the high-resolution studies include many more stars than shown

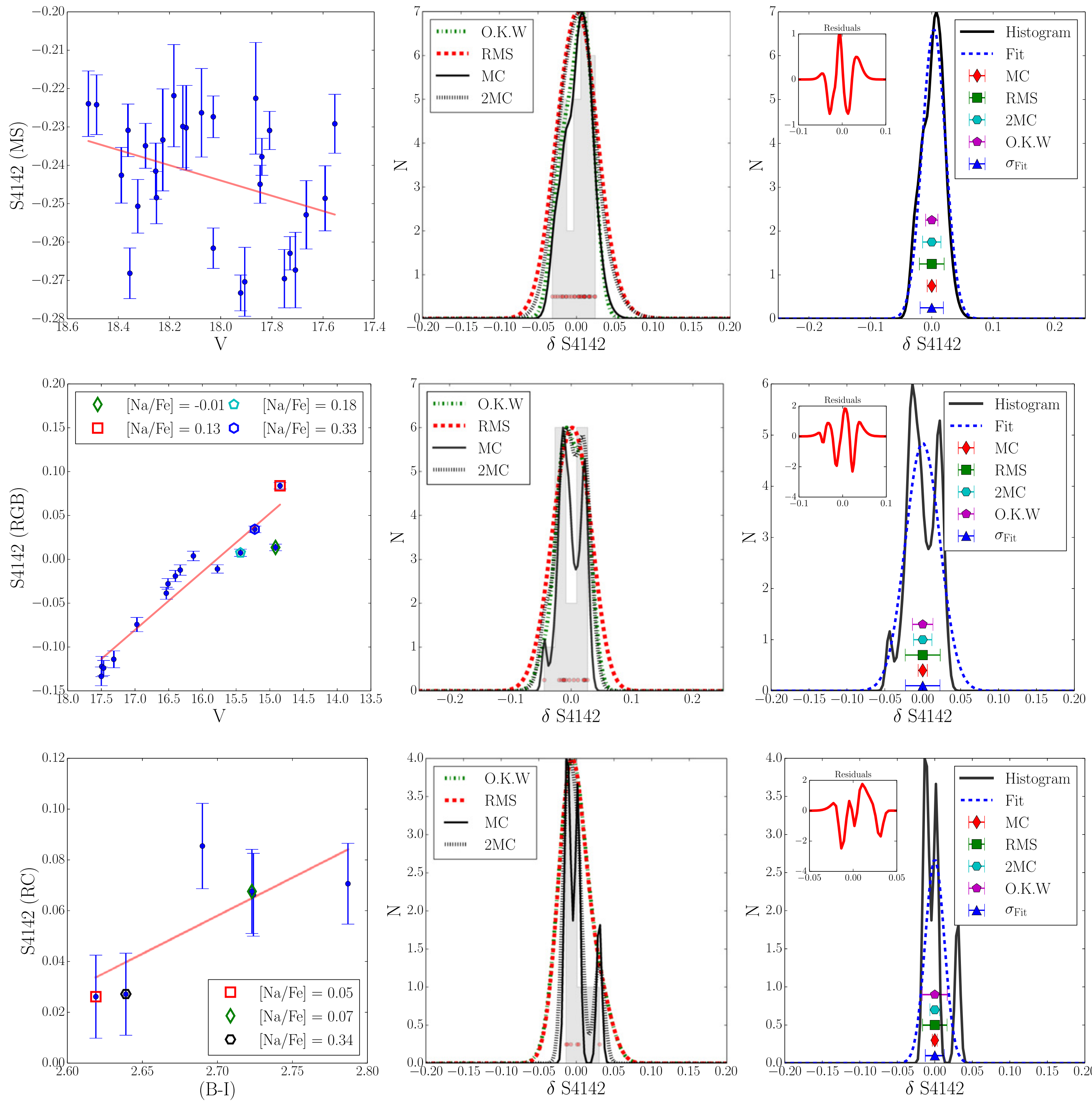

Figure 5. As in Figure 3, but for the $\delta S(4142)$ indices.

here, but these stars are not in the SEGUE sample. The majority of the stars in common between the high-resolution studies and our SEGUE sample are located near the tip of the RGB and in the RC. We have used these abundances to put further constraints on the behavior of the molecular band strengths in NGC 6791 using SDSS spectra.

In the first column of Figures 3–5 we mark the RGB and RC stars for which there are [Na/Fe] abundance measurements from Bragaglia et al. (2014) and Geisler et al. (2012), and give their values in the legend. If there were multiple populations in the cluster, one might expect the CN strength to correlate with [Na/Fe] abundances, with the Na-enhanced stars correlating with the stars with CN strengths above the linear fit, and Na normal stars correlating with stars below the fit. Although we have only six stars with [Na/Fe] in common with Bragaglia et al. (2014), they show no indication of a relationship between CN band strength and Na abundance. For NGC 6791, Bragaglia et al. (2014) measure $[C/Fe] \sim -0.12$, $[N/Fe] \sim +0.16$, and $[O/Fe] \sim -0.18$ ratios that are consistent with other OCs such as NGC 7789 (Tautvaišienė et al. 2005). Bragaglia et al. (2014) also do not find the signatures of two nitrogen populations in the cluster, which would lead one to expect that the molecular band strengths would be characteristic of a single population, contrary to what is found by Carrera (2012).

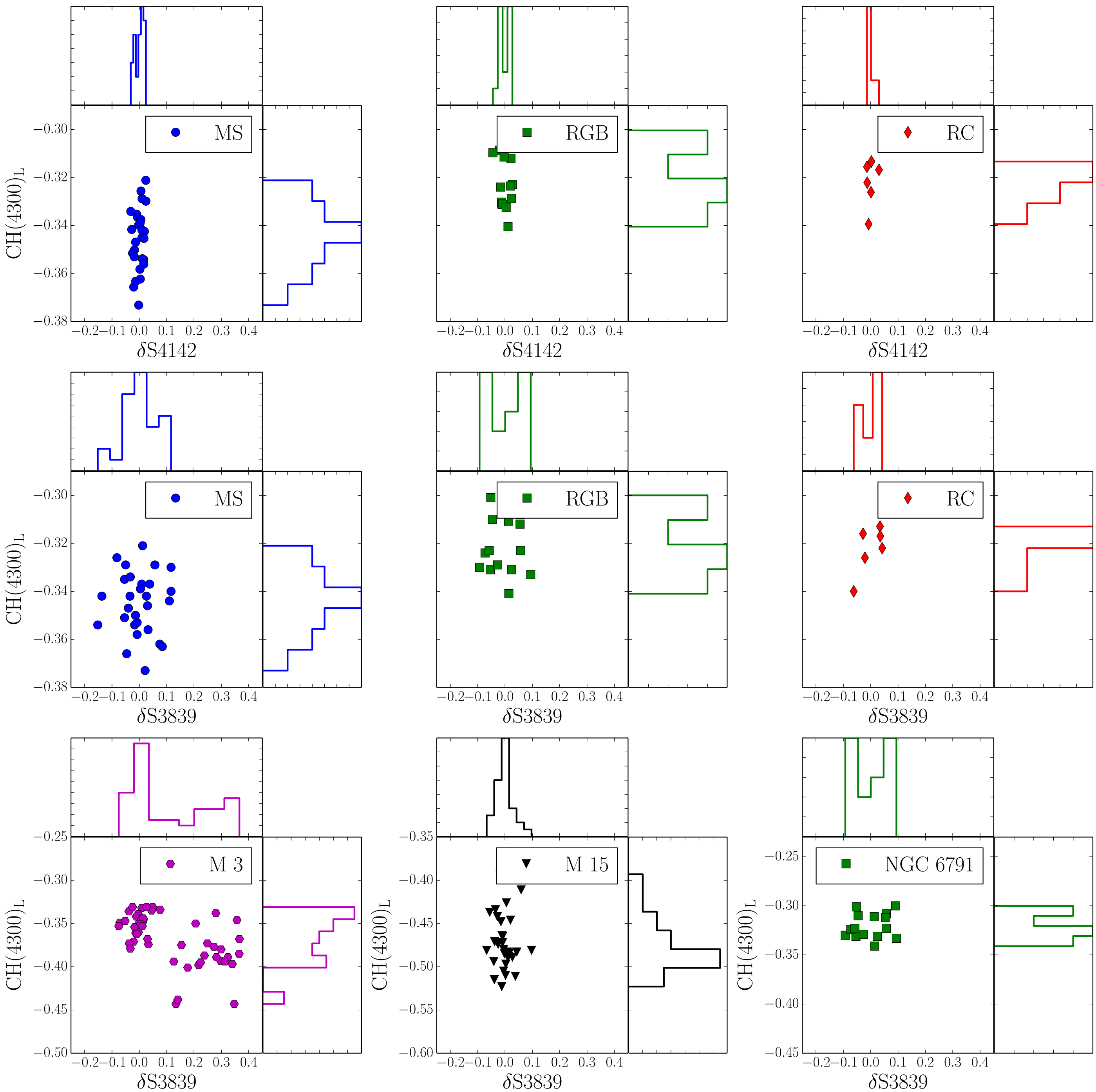

Figure 6. Top two rows: $CH(4300)_L$ vs. $\delta S(3839)_N$ and $CH(4300)_L$ vs. $\delta S(4142)$ for the MS, RGB, and RC in NGC 6791. Bottom row: $CH(4300)_L$ vs. $\delta S(3839)_N$ for RGB stars in M3, M15, and NGC 6791.

4.1. Synthetic Spectra Analysis

The CH and CN bands in GC stars have been used frequently to derive C and N abundances (e.g., Briley et al. 2004a, 2004b; Martell et al. 2008); we were interested in seeing how successful such techniques would be at estimating abundances from NGC 6791 spectra. The independently determined C and N abundances from Bragaglia et al. (2014) provided a means to test this approach. Following the approach of Briley et al. (2004a, 2004b), we used MARCS model atmospheres (Gustafsson et al. 1975) and the synthetic spectrum generator (SSG; Bell et al. 1994) to create synthetic spectra for each star. The carbon and nitrogen abundances used to generate the synthetic spectra are simultaneously adjusted to match both the $S(3839)_N$ and $CH(4300)_L$ observed for a star until a best fit is achieved. The best fit is the pair of [C/Fe] and [N/Fe] values that most closely reproduces the $CH(4300)_L$ and $S(3839)_N$ strengths measured in the observed spectra with those measured in the synthetic spectra. These best-fit values are then taken as the [C/Fe] and [N/Fe] values for a given star. For the synthetic spectra of RC stars in NGC 6791, we assumed atmospheric parameters that were typical of those

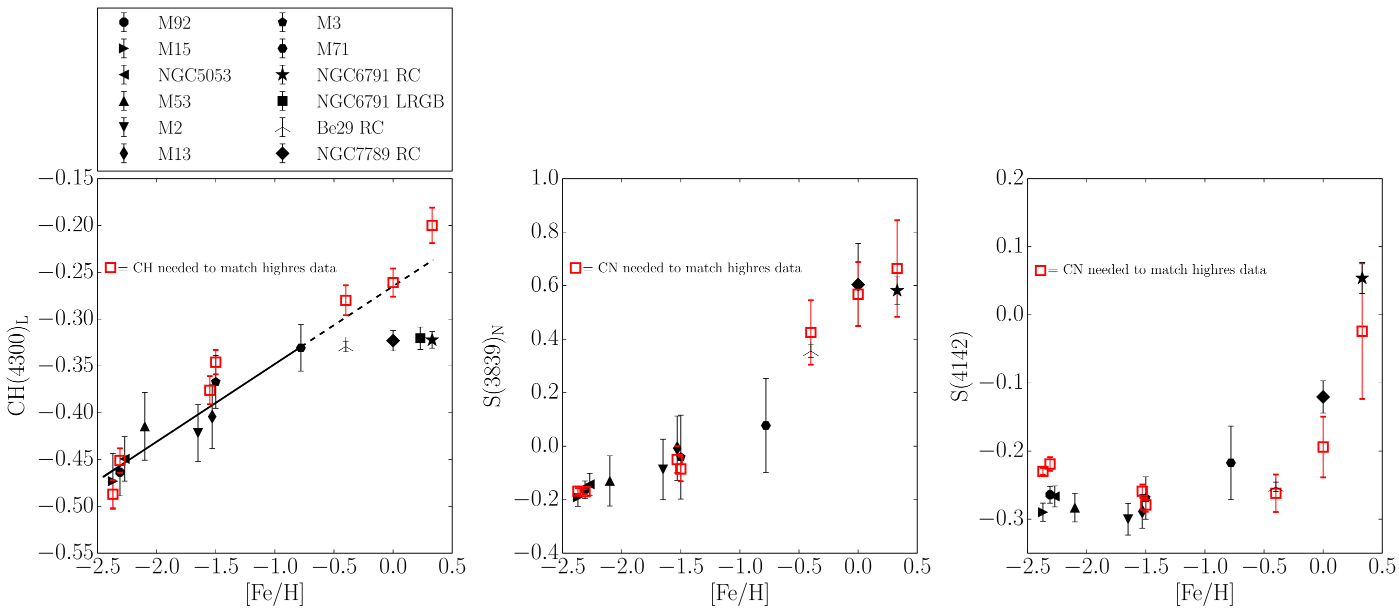

Figure 7. Left panel: plot of the average $CH(4300)_L$ band strength in RGB stars vs. [Fe/H] for a sample of GCs and OCs available in SEGUE. The black line is a linear fit to the $CH(4300)_L$ vs. [Fe/H] relation up to the M71. Middle panel: same as left panel, but for $S(3839)_N$ vs. [Fe/H]. Right panel: same as left panel, but for S(4142) band strength vs. [Fe/H]. The open red squares mark the locations of the $CH(4300)_L$, $S(3839)_N$, and S(4142) band strengths needed to match the [C/Fe] and [N/Fe] abundances in each cluster as reported by high-resolution studies. The vertical error bars on the red squares are explained in the text. The error bars on the black markers represent the standard deviation of the respective band strength distribution in each cluster.

found in Bragaglia et al. (2014) ([Fe/H] = +0.33, [O/Fe] = −0.18, $^{12}C/^{13}C = 20.0$, microturbulent velocity $(\xi) = 2.0\,\mathrm{km\,s^{-1}}$, effective temperature $(T_{\mathrm{eff}}) = 4500$ K, log $(g) = 2.5$ (cgs)). These were considered good assumptions for all RC stars due to the fact that there are only small variations observed in the stellar atmospheric parameters within the RC.

The [N/Fe] and [C/Fe] resulting from this process do not agree with the results from Bragaglia et al. (2014). The average [N/Fe] for the RC stars was very high at [N/Fe] = 2.0, while the [C/Fe] was far too low at [C/Fe] = −2.0 to −1.5. While some difference is expected (±0.2 dex) based on our assumptions of constant values for every star in parameters such as effective temperature and surface gravity, such a large discrepancy between the high-resolution abundance measurements and those from fitting low-resolution band strengths was not expected.

Suspecting that much of the problem lay in the very high metallicity of NGC 6791, we computed CN and CH band strengths for giant stars in two slightly less metal-rich OCs, NGC 7789 and Be 29, using the same method to evaluate their carbon and nitrogen abundances. The spectra for Be 29 and NGC 7789 were also taken from SEGUE, and the cluster membership was determined by Morrison et al. (2016). For NGC 7789 Tautvaišienė et al. (2005) measured [C/Fe] = −0.21 and [N/Fe] = +0.20 from high-resolution spectra. Be 29 does not have C and N abundances available, so we assumed that it would have [C/Fe] and [N/Fe] values similar to those in NGC 6791 and other OCs. For these clusters, we used an effective temperature of 4800 K and a log(g) of 2.5 for all stars based on their lower metallicities. For NGC 7789, we used [Fe/H] = 0.0, $^{12}C/^{13}C = 9.0$, and $\xi = 2.0\,\mathrm{km\,s^{-1}}$ based on data from Tautvaišienė et al. (2005). For Be 29, we adopted [Fe/H] = −0.4 (Carrera & Pancino 2011), $^{12}C/^{13}C = 10$, and $\xi = 2.0\,\mathrm{km\,s^{-1}}$, typical of red clump stars. Again, the resulting [N/Fe] and [C/Fe] abundances based on the $S(3839)_N$ and $CH(4300)_L$ measurements did not match the high-resolution work, with over-enhanced nitrogen and overdepleted carbon. We will explore why the [N/Fe] and [C/Fe] abundances determined from band strengths in synthetic spectra did not match high-resolution abundance measurements in the next section.

4.2. *Saturating* $CH(4300)_L$ *Band Strength*

To explore the behavior of the $CH(4300)_L$ band strength at high metallicities, we collected a sample of $CH(4300)_L$ measurements in GCs of a range of metallicities from Smolinski et al. (2011). The left panel of Figure 7 shows the mean observed $CH(4300)_L$ band strengths of the RGB stars in each of the clusters versus their [Fe/H] values. The mean $CH(4300)_L$ band strength in the cluster RGB samples increases with cluster [Fe/H] until reaching M71 at a metallicity of [Fe/H] = −0.78. Beyond this metallicity the mean $CH(4300)_L$ band strength stays approximately constant up to the metallicity of NGC 6791 at [Fe/H] = +0.33, a clear indication of the saturation of the CH band.

The behavior of CH(4300) with metallicity below [Fe/H] ~ −0.7 appears roughly linear and, extrapolated to higher metallicities, suggests how much weaker the measured OC CH band strengths might be than expected. To test this notion, we ran the SSG to create synthetic spectra at the metallicities of Be 29, NGC 7789, and NGC 6791 with the carbon and nitrogen abundances found by the high-resolution studies where they are available (Tautvaišienė et al. 2005; Bragaglia et al. 2014). Using these synthetic spectra, we found a theoretical $S(3839)_N$, S(4142), and $CH(4300)_L$ band strength for each cluster, i.e., what the models would predict these values would be for a star at the given metallicity, effective temperature, surface gravity, [O/Fe], [C/Fe], and [N/Fe] in each cluster. These theoretical $CH(4300)_L$ values are plotted as open red squares in Figure 7, and we see that they fall very close to the values predicted by the linear trend defined by the more metal-poor clusters. This clearly demonstrates the saturation of the $CH(4300)_L$ band at higher metallicities and its lack of utility for determining C abundances in metal-rich clusters.

To provide more insight into the discrepancies between the measured $CH(4300)_L$ molecular band strengths and their predicted values, we then created synthetic spectra for four GCs from the SEGUE sample to compare their theoretical $CH(4300)_L$, $S(3839)_N$, and S(4142) band measurements with the average observed measured indices from the SEGUE data. To create the synthetic spectra, we adopted [Fe/H] values from the Harris catalog and assumed an [O/Fe] of 0.3 dex, $^{12}C/^{13}C = 4.0$, and a microturbulent velocity of 2.0 km s^{-1} for all four clusters. Values for $T_{\rm eff}$, log(g), [C/Fe], and [N/Fe] were taken from Suntzeff (1981) for M3 and M13, from Carbon et al. (1982) for M92, and from Trefzger et al. (1983) for M15. These abundances are determined from direct spectral synthesis and matching of individual stellar spectra, not the modeling of spectroscopic indices used here. We found that the theoretical $CH(4300)_L$, $S(3839)_N$, and S(4142) band measurements for these four metal-poor clusters (shown as red squares in Figure 7) are in good agreement with the average measurements taken from the SEGUE data. This expected result supplied further evidence that the method does work for GCs, and is therefore only a problem at higher metallicities due to the saturation of the $CH(4300)_L$ band.

To evaluate the uncertainties of the band strengths produced by the model, we calculated the band strengths with changes in the assumed temperature ([O/Fe], [C/Fe], and [N/Fe]) of ± 100 K and 0.1 dex in each abundance. The differences in band strengths caused by these factors were then added in quadrature to determine an estimate for the uncertainty of each band, indicated by the red error bars in Figure 7. As expected, the uncertainty in a given band strength increases with metallicity, but the uncertainty in the CH band is not large enough to explain the difference seen between the models and the observed band strengths at high metallicity.

While we do not have an explanation for the large disparity between the predicted and the observed G-band strengths, the fact that the models diverge increasingly from the observations with increasing metallicity suggests that the reason is related to the increased opacity and very cool temperatures found in the metal-rich giants in the OCs. The G band is known to be insensitive to changes in overall metallicity (Faber et al. 1985). In spite of the fact that the G band appears to be an unreliable indicator of C abundance at high metallicities, we find very different behavior in the $S(3839)_N$ and S(4142) CN indicies. The middle and right panels of Figure 7 show that the observed and predicted $S(3839)_N$ and S(4142) index values for the sample of GCs and OCs are in reasonable agreement throughout the metallicity range. This is especially true for the $S(3839)_N$ band. While the S(4142) band does not have the same level of agreement between the observed and modeled values, the models do follow the general trend of increasing S(4142) strength with metallicity above [Fe/H] ~ -0.7. This agreement leads us to have confidence in the ability of the $S(3839)_N$ and S(4142) index to reflect underlying differences in N abundances even at the high metallicities of NGC 6791.

5. SIMULATING BAND STRENGTH DISTRIBUTIONS

In order to have a more thorough understanding of the band strength distributions, we created a simulation of what would be observed in a cluster with two distinct nitrogen populations. To accomplish this, we used the MARCS model atmospheres and the SSG code to generate synthetic spectra with given [N/Fe] and [C/Fe] distributions. The $S(3839)_N$, $CH(4300)_L$, and S(4142) band strengths are then measured from these synthetic spectra. This allowed us to simulate what we would observe in molecular band strengths if an N-normal and N-strong population were indeed present in the cluster. Typical abundance differences of $\sim$1.0 dex in [N/Fe] and $\sim$0.5 dex in [C/Fe] are seen between stellar generations in GCs (Briley et al. 2004a), but we can expect that enhancements in N would decrease with increasing metallicity. Predicted asympotic giant branch (AGB) yields by Ventura et al. (2002) indicate that at [Fe/H] $= -0.3$ ejecta from a five solar mass AGB star would give depletions of [C/Fe] $= -1.1$ and enhancements of [N/Fe] $= +0.7$, relative to the initial abundances. While that study does not reach the high metallicity of NGC 6791, there is a general trend that [N/Fe] enrichment decreases with increasing metallicity. Therefore, we do not know exactly what the yields would be in NGC 6791, but an enhancement of +0.5 dex in [N/Fe] is consistent with that trend.

To simulate what would be observed in a cluster like NGC 6791, we created two Gaussian distributions in [N/Fe], one centered at the expected [N/Fe] of NGC 6791 and another 0.5 dex stronger, each with a standard deviation of 0.1 dex. Then we randomly drew six stars from the $S(3839)_N$ distribution produced by these two [N/Fe] populations. We calculated the standard deviation of these six $S(3839)_N$ band strength measurements and repeated this experiment 1000 times. We chose six as our sample size to reflect the number of RC stars available in the SEGUE data. We then compared the most probable standard deviation of these experiments to what is actually observed in the six RC stars in NGC 6791. The results of these simulations are shown in Figure 8. In the first panel of the top row, we plot the $S(3839)_N$ distribution that results from the two Gaussian [N/Fe] distributions described above. Each of the panels in Figure 8 is labeled with the characteristics of the [N/Fe] populations used in creating the simulated CN distributions. For comparison, the second panel in this row is the $\delta S(3839)_N$ distribution for M3 as measured by Smolinski et al. (2011). In the last panel, we plot the probability density functions (PDFs) of the standard deviation values (σ) of the samples randomly drawn from the simulated and M3 distributions. The PDF of the simulated data is plotted as a red line, and the PDF of the M3 data is plotted as a green line. The solid blue line marks the location of the measured standard deviation of $\delta S(3839)_N$ values from the six RC stars in our sample. The solid black line marks the average standard deviation of six $\delta S(3839)_N$ measurements randomly selected from the M3 distribution, and the dotted black line marks the location of standard deviation of the entire $\delta S(3839)_N$ sample in M3. From this simulation, we see that the measured standard deviation of the $S(3839)_N$ band strengths in NGC 6791 is much smaller than the average σ value from our simulation. In fact, there is only an $\sim$4% chance that six $S(3839)_N$ band strengths drawn from this simulation would have a standard deviation less than that in the RC stars of NGC 6791. In M3, a cluster known to have two distinct nitrogen populations, the typical standard deviation of six stars randomly drawn from the CN data had a value that was nearly identical to the actual standard deviation of the entire M3 sample, suggesting that it is possible to detect the two populations from a sample of six stars.

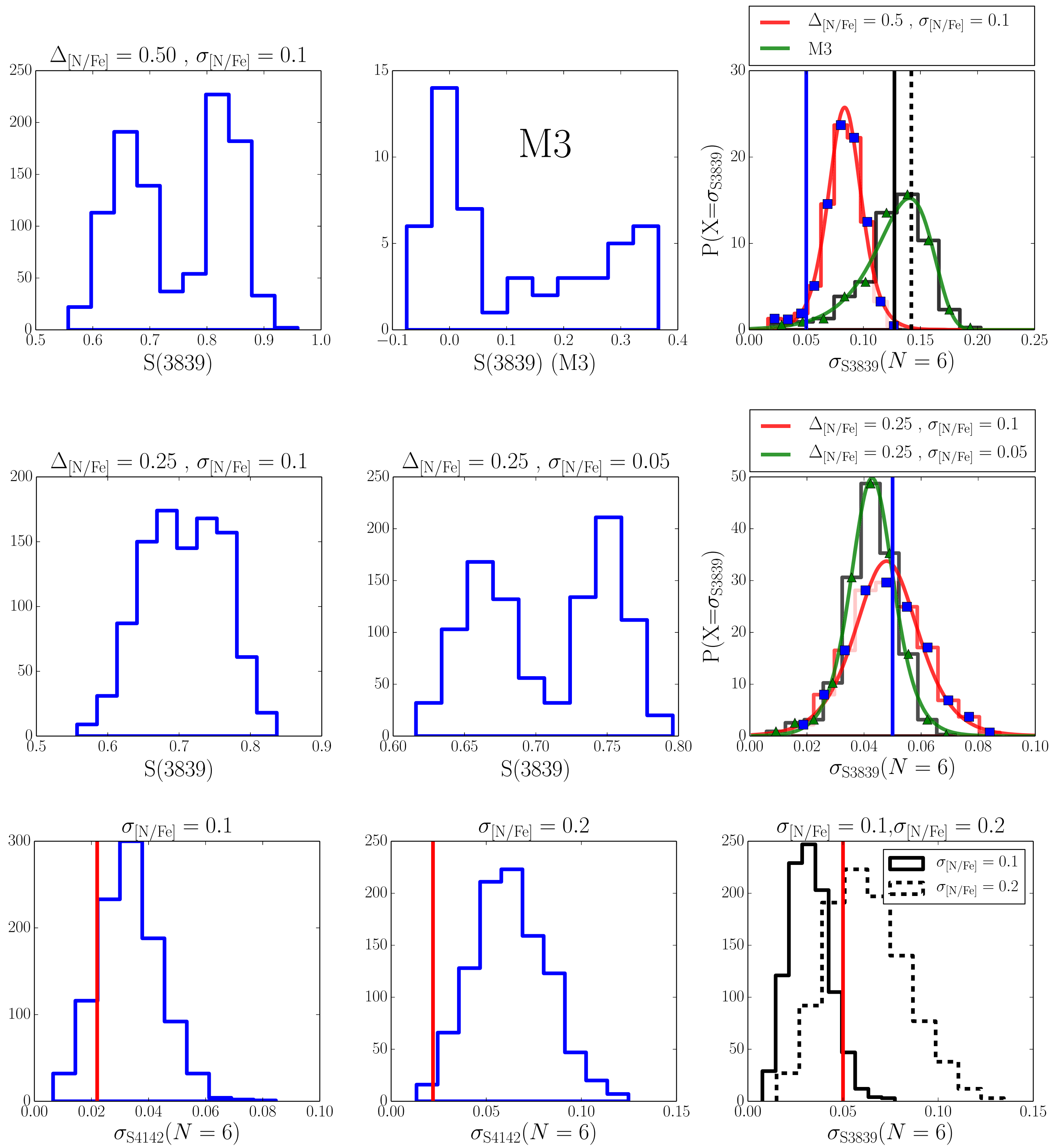

Figure 8. Plot of the CN distributions resulting from two Gaussian [N/Fe] populations, one normal and one strong. In the first two rows each panel is labeled with two values, $\Delta_{[N/Fe]}$ and $\sigma_{[N/Fe]}$, where $\Delta_{[N/Fe]}$ is the separation between the mean values of the [N/Fe] Gaussians, and the $\sigma_{[N/Fe]}$ is their standard deviations. The first two panels in each row show the CN distributions resulting from the [N/Fe] Gaussians with the characteristics given in their titles. In the second panel of row 1 we plot the observed δ CN distribution of the GC M3 for comparison. In the last panel of the first two rows we plot the PDF of the standard deviation of six stars randomly drawn from the two CN distributions in the previous panels. The solid blue vertical line marks the location of the measured standard deviation of the six CN measurements from the RC stars in NGC 6791. The solid black line marks the mean standard deviation of six stars randomly drawn from the M3 sample, and the dashed line marks the location of the standard deviation of the entire M3 sample. The final row plots the standard deviation distributions resulting from single [N/Fe] populations with the σ values given in the title.

To place limits on the likelihood of detecting different N populations in a cluster like NGC 6791, we ran additional simulations in which the two nitrogen populations were chemically closer together. In each of these simulations the nitrogen strong population was only enhanced +0.25 dex in [N/Fe] relative to the nitrogen normal population. The width of each of the Gaussian distributions was adjusted to explore how narrow these underlying abundance distributions would have to be in order to see a separation between the two populations. The middle row in Figure 8 shows the results of adopting widths of 0.1 and 0.05 dex. In the last panel of this row the blue line marks the measured standard deviation of the $\delta S(3839)_N$ values in NGC 6791 RC stars. From this panel, we see that the typical standard deviation of six randomly selected $\delta S(3839)_N$ values is much closer to the measured value in NGC 6791 when the two nitrogen populations are only separated by 0.25 dex and have widths of 0.1 dex. We conclude that the existing $S(3839)_N$ data do rule out any discrete [N/Fe] populations that differ by more than ~0.25 dex.

The tests illustrated in the first two rows were also performed with the nitrogen-enhanced population only making up 20% of the total stellar population. Changing the ratios of the populations, however, did not create drastic differences in the standard deviation distributions resulting from randomly drawing 6 $S(3839)_N$ values from the sample.

We can also use the S(4142) band, because of its smaller observed dispersion, to provide additional constraints on the N abundance distribution in NGC 6791. Using the same model above, with each of the [N/Fe] populations separated by 0.25 dex and with widths of 0.1 dex, the expected standard deviation of six randomly drawn S(4142) values is a factor of 2–3 larger than what is actually observed. Unable to reproduce the measured standard deviation seen in the S(4142) band with two separate N populations, we repeated these simulations with a single [N/Fe] Gaussian distribution.

The results are shown in the first two panels of the final row of Figure 8. In the first and middle panel, we plot the standard deviation distributions of six S(4142) values resulting from a single [N/Fe] population with sigma = 0.1 and 0.2, respectively. The vertical red line marks the measured standard deviation of the six S(4142) values in the NGC 6791 RC stars. We see that a single Gaussian distribution in [N/Fe] with sigma = 0.1 most closely reproduces the measured S(4142) standard deviation. In the final panel of the row, we plot the results of this test for the $S(3839)_N$ band, where we see that a single population also nearly reproduces the measured $S(3839)_N$ standard deviation, although sigma = 0.2 more closely matches the observed value.

We note, though, that none of these comparisons have taken into account the observational errors on the measured indices. These are expected to be larger for $S(3839)_N$ than for S(4142) due to the lower flux in the blue, a result of the cool temperatures of these stars and the heavy line blanketing, especially at the metallicity of NGC 6791. This results in appreciably lower S/N values at the location of $S(3839)_N$ than at S(4142), and associated larger measurement errors. Considering that the intrinsic dispersion in $\delta S(3839)_N$ would be smaller than that observed suggests that the limitations on the underlying abundance distribution of N from the $S(3839)_N$ and the S(4142) band are not inconsistent. We conclude that the variation in [N/Fe] in NGC 6791 is at most 0.2 dex and may be as small as 0.1 dex.

6. DISCUSSION AND CONCLUSIONS

From our analysis of the $S(3839)_N$, S(4142), and $CH(4300)_L$ distributions in NGC 6791, we find that there is not conclusive evidence that they show signs of light-element variations or signatures of multiple populations. With the limited number of stars available in the RGB and RC of the cluster, it is difficult to create robust determinations of the shapes and characteristics of the distributions. This difficulty is amplified by how one decides to assign errors to the band strength measurements. As we illustrated in the generalized histograms in Figures 3–5, with so few stars, the final conclusions one can draw about these distributions rely almost entirely on how the errors are determined.

Comparing the values in Table 1, we see that the generalized histograms resulting from the unsmoothed MC errors are always wider than the median error, suggesting abundance variations in the cluster. From the unsmoothed MC error values alone, it would appear that the distributions are approximately two times wider than they should be based on the errors. The optimal kernel width method also resulted in some very small errors in the cases of the RGB and RC samples, but this is likely due to the relatively small number of stars available in those samples. This conclusion is supported by the fact that the errors for the RC sample with only six stars are even smaller than those for the larger RGB sample stars, though their spectra are of similar S/N. If we assume that the $S(3839)_N$ errors should match what is adopted for other studies, a value of 0.05, then the width of the $S(3839)_N$ distributions would be more consistent with the errors in the measurements. If we examine the linear fits to the band strengths in Figures 3 and 4, they appear to be somewhat meaningless, especially for the $S(3839)_N$ strengths in the RGB and RC assuming unsmoothed MC errors. In these cases it is hard to assess what the generalized histograms of the pseudo-indices will be able to tell us, especially with so few stars. The RC distribution in each of the bands has the strongest hints of what could be a double-peaked distribution. This structure, however, is the result of a single star that appears to be an outlier from the rest of the RC sample. When we remove this star, which is the bluest of the RC sample, and re-create the generalized histograms, they clearly form a single peak.

By using synthetic spectra, we have been able to explore the behavior of the $CH(4300)_L$, $S(3839)_N$, and S(4142) bands at the solar and supersolar metallicities found in Be 29, NGC 7789, and NGC 6791. Our analysis has shown that the strength of the observed $CH(4300)_L$ band is very similar in these three clusters, contrary to the increasing band strength predicted from synthetic spectra computed using the abundances determined from high-resolution studies. The strength of the $S(3839)_N$ band, however, is observed to increase approximately linearly through the entire range of [Fe/H] values, as shown by Figure 7, consistent with predictions of synthetic spectra. We also find generally good agreement between the modeled S(4142) values and what is measured in the GCs and OCs. Assuming, then, that the observed CN strength successfully tracks the N abundance even at high metallicity, we use the CN bands to put constraints on the N abundance variations in NGC 6791.

Using synthetic spectra, we simulated the $S(3839)_N$ and S(4142) distributions that would be produced in a cluster with two distinct [N/Fe] populations, and what one would observe with sample sizes similar to those in NGC 6791. From this simulation, we found that the scatter of the $S(3839)_N$ band strengths in the six RC stars in NGC 6791 is statistically unlikely to be due to a population with two [N/Fe] populations separated by 0.5 dex. In order to match the observed dispersion among RC stars in NGC 6791, the two populations would have to be separated by no more than 0.25 dex in [N/Fe], with widths on the order of 0.1 dex. The small observed dispersion in the S(4142) band places more stringent limitations; we are able to reproduce the observed dispersion with a single [N/Fe] distribution with an intrinsic variation of no more than 0.1 dex. We conclude that the variation in the underlying [N/Fe] distribution in NGC 6791 is at most 0.2 dex and may be less than 0.1 dex.

From our analysis of the $S(3839)_N$, S(4142), and $CH(4300)_L$ band strengths in NGC 6791, with the addition of synthetic spectral analysis made possible by high-resolution work, we do not find the cluster to show chemical inhomogeneities. Perhaps more importantly, we conclude that the CH molecular band strengths may not be sensitive enough to detect these chemical variations in higher-metallicity systems, such as OCs. This suggests that there is a metallicity sweet spot ($-2.10 \lesssim$ [Fe/H] $\lesssim -0.7$) where this technique is sensitive to determine the C and N abundances of multiple populations.

We would like to thank Roger A. Bell for making the SSG program available to us. We would also like to thank the referee for their useful comments that helped improve the paper. This material is based on work supported by the National Science Foundation Graduate Research Fellowship Program under Grant No. DGE-1342962 to O.M.B. Any opinion, findings, and conclusions or recommendations expressed in this material are those of the author(s) and do not necessarily reflect the views of the National Science Foundation.

REFERENCES

Anthony-Twarog, B. J., & Twarog, B. A. 1985, ApJ, 291, 595
Bell, R. A., Paltoglou, G., & Tripicco, M. J. 1994, MNRAS, 268, 771
Bragaglia, A., Sneden, C., Carretta, E., et al. 2014, ApJ, 796, 68
Briley, M. M., Cohen, J. G., & Stetson, P. B. 2004a, AJ, 127, 1579
Briley, M. M., Harbeck, D., Smith, G. H., & Grebel, E. K. 2004b, AJ, 127, 1588
Briley, M. M., Smith, G. H., Bell, R. A., Oke, J. B., & Hesser, J. E. 1992, ApJ, 387, 612
Brogaard, K., VandenBerg, D. A., Bruntt, H., et al. 2012, A&A, 543, A106
Carbon, D. F., Romanishin, W., Langer, G. E., et al. 1982, ApJS, 49, 207
Carrera, R. 2012, ApJ, 758, 110
Carrera, R., & Pancino, E. 2011, A&A, 535, A30
Carretta, E., Bragaglia, A., Gratton, R., & Lucatello, S. 2009, A&A, 505, 139
Carretta, E., Bragaglia, A., Gratton, R. G., et al. 2010, A&A, 516, A55
Cunha, K., Smith, V. V., Johnson, J. A., et al. 2015, ApJL, 798, L41
Faber, S. M., Friel, E. D., Burstein, D., & Gaskell, C. M. 1985, ApJS, 57, 711
Friel, E. D., & Janes, K. A. 1993, A&A, 267, 75
Geisler, D., Villanova, S., Carraro, G., et al. 2012, ApJL, 756, L40
Gratton, R., Bragaglia, A., Carretta, E., & Tosi, M. 2006, ApJ, 642, 462
Gratton, R. G., Carretta, E., & Bragaglia, A. 2012, A&AR, 20, 50
Gustafsson, B., Bell, R. A., Eriksson, K., & Nordlund, A. 1975, A&A, 42, 407
Hufnagel, B., Smith, G. H., & Janes, K. A. 1995, AJ, 110, 693
Kaluzny, J., & Udalski, A. 1992, AcA, 42, 29
King, I. R., Bedin, L. R., Piotto, G., Cassisi, S., & Anderson, J. 2005, AJ, 130, 626
Kraft, R. P. 1994, PASP, 106, 553
Lee, S.-G. 1999, AJ, 118, 920
Liebert, J., Saffer, R. A., & Green, E. M. 1994, AJ, 107, 1408
Martell, S. L., & Grebel, E. K. 2010, A&A, 519, A14
Martell, S. L., Smith, G. H., & Briley, M. M. 2008, PASP, 120, 839
Morrison, H. L., Ma, Z., Clem, J. L., et al. 2016, AJ, 151, 7
Norris, J., Cottrell, P. L., Freeman, K. C., & Da Costa, G. S. 1981, ApJ, 244, 205
Norris, J., & Freeman, K. C. 1979, ApJL, 230, L179
Peterson, R. C., & Green, E. M. 1998, ApJL, 502, L39
Platais, I., Cudworth, K. M., Kozhurina-Platais, V., et al. 2011, ApJL, 733, L1
Shetrone, M., Martell, S. L., Wilkerson, R., et al. 2010, AJ, 140, 1119
Smith, G. H. 1987, PASP, 99, 67
Smolinski, J. P., Martell, S. L., Beers, T. C., & Lee, Y. S. 2011, AJ, 142, 126
Stetson, P. B., Bruntt, H., & Grundahl, F. 2003, PASP, 115, 413
Suntzeff, N. B. 1981, ApJS, 47, 1
Tautvaišienė, G., Edvardsson, B., Puzeras, E., & Ilyin, I. 2005, A&A, 431, 933
Trefzger, D. V., Langer, G. E., Carbon, D. F., Suntzeff, N. B., & Kraft, R. P. 1983, ApJ, 266, 144
Tripicco, M. J., Bell, R. A., Dorman, B., & Hufnagel, B. 1995, AJ, 109, 1697
Twarog, B. A., Carraro, G., & Anthony-Twarog, B. J. 2011, ApJL, 727, L7
Ventura, P., D'Antona, F., & Mazzitelli, I. 2002, A&A, 393, 215
Yanny, B., Rockosi, C., Newberg, H. J., et al. 2009, AJ, 137, 4377